ELSEVIER

Journal of Nuclear Materials 266–269 (1999) 1129–1133

journal of nuclear materials

Finite element modelling D_α radiation and impurity transport in tdev

R. Marchand *, F. Meo, M. Simard, B. Stansfield, E. Haddad, G. Abel, J.L. Lachambre, D. Pinsonneault, N. Richard, TdeV team

Centre Canadien de Fusion Magnéique 1804 boul. Lionel Boulet, Varennes Qc J3X 1S1, Canada

Abstract

Particle and energy transport are modelled in TdeV using the multispecies finite element simulation code TOPO. For every charged species, equations are solved for the conservation of particles, parallel momentum, and energy. For neutral species, equations are solved for the conservation of particles and energy. For simplicity, all neutral fluxes are assumed to be diffusive. The transport equations are discretised with finite elements on a triangular unstructured mesh. This allows a realistic description of the TdeV divertor geometry, with segmented divertor plates arbitrarily oriented with respect to the local flux surfaces. The use of an unstructured mesh also allows local mesh refinement in the vicinity of the X point, and at selected locations near the divertor plates. Comparisons between simulated and experimentally measured density profiles are presented. Detailed comparisons between calculated and measured D_α specific intensities are also presented. Finally, an assessment is made of the single ion temperature approximation commonly made in other edge transport models.

Keywords: 2D modeling; Carbon impurities; Hα emission

1. Introduction

Computer modelling of tokamak plasmas is a powerful tool for interpreting experiments and is necessary for extrapolating present knowledge. The main challenge in developing a useful model is to consistently account for a large number of coupled physical processes in a calculation, while rendering quantitative results under realistic experimental conditions. A number of approaches are being used for that purpose, as described in Refs. [1–5]. The principal difference between our approach and the others cited is in the use of a finite element discretisation of the transport equations, on an unstructured triangular mesh. The latter provides a significant advantage in setting up a realistic representation of an experiment.

In the following, the multi-fluid finite element code TOPO is used to simulate the edge and divertor plasmas for a variety of TdeV operating conditions. In particular, the plasma density profile is calculated in the edge in the equatorial plane, and compared with probe measurements. Two dimensional emissivity profiles are also calculated for D_α radiation. Their integration along specified lines of sight are compared directly with experimental measurements. The code is also used to calculate the ion temperature under a variety of recycling conditions. Ion temperatures are not readily measured experimentally, and a comparison with experiment is unfortunately not possible. A calculation of T_i is nonetheless of interest, because of the importance of thermal forces in impurity transport [6,7]. Most other transport models assume instantaneous equilibration among all ions species into a single ion temperature. In the present model, an energy conservation equation is solved for every ion species and, thus, each species has a distinctive temperature. This makes it possible to assess the validity of the single ion temperature hypothesis.

* Corresponding author. Tel.: +1-450 652 8866; fax: +1-450 652 8625; e-mail: marchand@ccfm.ireq.ca.

0022-3115/99/$ – see front matter
PII: S0022-3115(98)00877-0

2. Model description

The physical and mathematical models used in the simulations have been described elsewhere [5]. They are briefly outlined here for completeness. Plasma and neutral transport are treated in the fluid approximation. The dynamics of every charged species is governed by three conservation equations; one for particles, one for parallel momentum and one for energy. All fluxes in the direction parallel to the magnetic field lines are assumed to be classical [8], while diffusion in the direction perpendicular to the magnetic field is assumed to be anomalous, with adjustable transport coefficients. The transport of neutral particles is treated in the diffusion approximation. More specifically, for every neutral species, only two conservation equations are solved, for particle mass and energy. Particle and energy fluxes are assumed to be proportional to local density and temperature gradients respectively. For simplicity, only atomic species are taken into account. The neglect of molecular species should be acceptable whenever the molecules released near the divertor plate, are dissociated and ionized very near to where they are produced. Finally, **E B** and diamagnetic drifts are not included in any of the transport equations. This is justified by earlier studies which indicated that they do not have a strong influence on most profiles [5]. All atomic rates used in the simulations are obtained from a collisional radiative model [9].

A complete definition of the problem also requires a set of boundary conditions. We distinguish between three types of boundaries: (1) divertor plates, (2) the boundary between the central plasma and the edge and (3) the outermost flux surfaces in the private region and in the edge. Standard sheath conditions are applied at the divertor plates [5]. At the boundary between the edge and the central plasma, we use essential conditions for the electron and ion temperatures; i.e., T_e and T_i are fixed. The density of deuterium ions and, for carbon impurities, the density of the highest ionisation stage considered (CV in all simulations) are also fixed. In all the cases considered, we use $n_{CV} = 0.01\ n_{DII}$ on that boundary. This is to account for highly ionised carbon species which diffuse from the high temperature core to the edge. Low ionisation stage carbon is also produced directly at the divertor by physical and chemical sputtering. For simplicity, a fixed 2% total sputtering yield is assumed for incident deuterium.

3. Simulation results

Results are now presented for two TdeV geometries. The first, referred to as TdeV95, corresponds to the machine as it was until 1995. The second, TdeV96, corresponds to the present divertor in TdeV. The interest in TdeV95 comes from the availability of more complete measurements of the D_α radiation profile. That geometry indeed allowed a tangential view of the outer divertor region which served to record full 2D distributions of the D_α specific intensity. The two geometries are illustrated in Figs. 1 and 2. In both cases, results are presented for a set of three densities (n_0) and tempera-

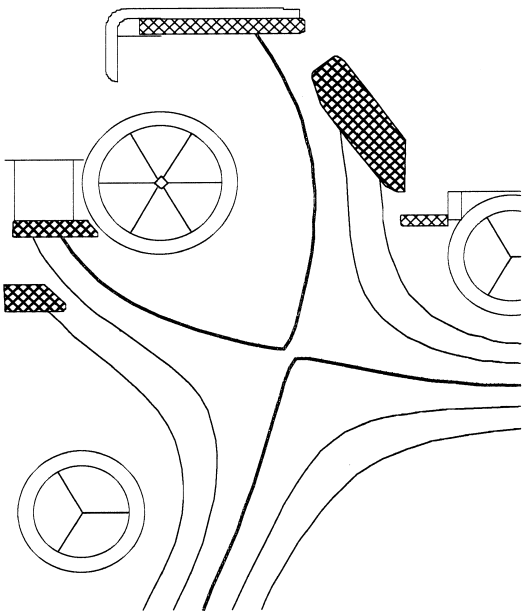

Fig. 1. Illustration of the TdeV95 geometry.

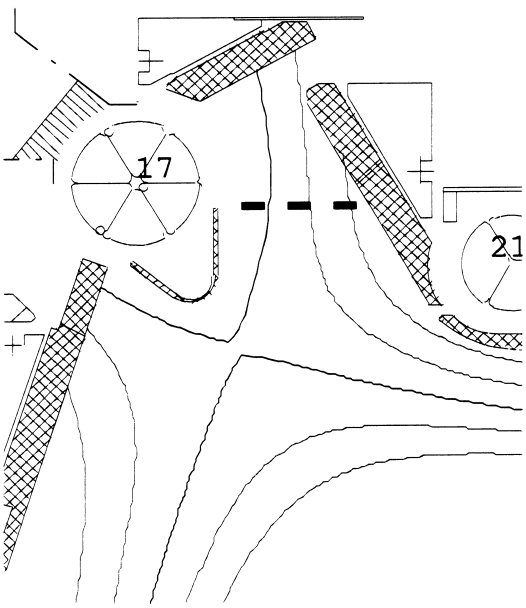

Fig. 2. Illustration of the TdeV96 geometry.

tures ($T_{e0} = T_{i0} = T_0$) at the boundary with the central region, corresponding to a power coming from the centre of approximately $P_0 \sim 90$ kW for TdeV95 and $P_0 \sim 80$ kW for TdeV96. The numerical values of the boundary conditions, the anomalous transport coefficients used in the simulations and the corresponding powers coming from the central plasma are summarised in Table 1. With the boundary between the edge and the central plasma being approximately 1cm inside the separatrix in the outer equatorial plane, n_0 is approximately 0.8 times the line average density measured along a vertical line of sight passing through the magnetic axis.

4. TdeV95 – D_α line radiation profile

For each of the three boundary conditions listed in Table 1, the D_α emissivity is calculated and the corresponding specific intensity is integrated over an array of lines of sight which corresponds to the camera's viewing configuration used to register the Dα radiation in the outer divertor. A direct comparison with unprocessed experimental measurements can thus be made. Because of the uncertainty in matching the imposed density at the boundary, n_0, with the experimentally measured line average density, a precise quantitative comparison is difficult. Some general dependencies on density can, nonetheless be determined. As an illustration, Fig. 3 shows the D_α emissivity profile calculated for the intermediate density ($n_0 = 2 \times 10^{19}$ m^{-3}). The corresponding calculated specific intensity profile, as would be seen from the camera is shown in Fig. 4. For comparison, Fig. 5 shows a measured specific intensity profile corresponding to a low density ($\bar{n}_e = 2.3 \times 10^{19}$ m^{-3}). In both cases, the general shape of the radiation profile is similar. For these low densities, the plasma is attached to the upper divertor plate, and the maximum radiation is found at the plate. Moreover, the numerical values of the specific intensities are comparable. A more detailed comparison between the calculated and measured D_α radiation profiles is presented in Fig. 6. There, the maximum specific intensities in a horizontal plane, are plotted as a function of the Z coordinate of that plane. At low density, the maximum intensity is found near the divertor plate. Also, in both cases, the region of maximum radiation moves away from the plate as density increases.

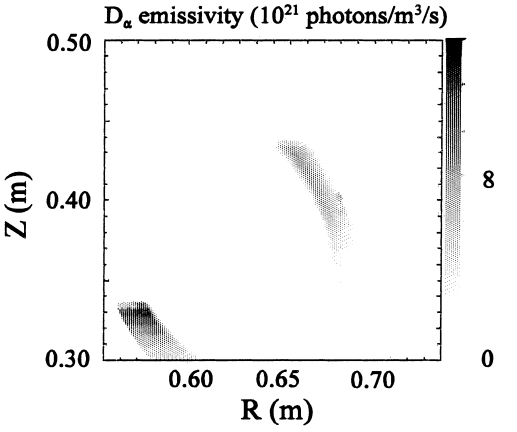

Fig. 3. Calculated D_α emissivity for $n_0 = 2 \times 10^{19}$ m^{-3}.

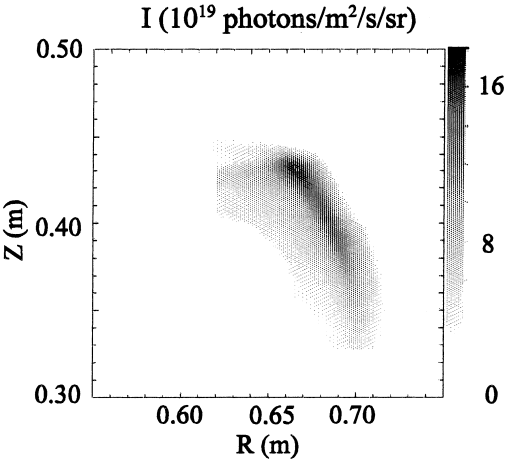

Fig. 4. Specific D_α intensity calculated for the camera viewing configuration, with $n_0 = 2 \times 10^{19}$ m^{-3}.

5. TdeV96 – Density and ion temperature profiles

Simulations have been made for three densities in TdeV96 geometry, corresponding to a power from the

Table 1
Summary of the parameters used in the simulations

Parameter scan		TdeV95			TdeV96		
	n_0 (10^{19} m^{-3})	1	2	4	1	2	4
	T_0 (eV)	100	60	31	150	100	60
Transport coefficients	$D_{i\perp}$ (m^2/s)	0.4 ∀i			Particle diffusivity		
	$\chi_{e\perp}/n_e$ (m^2/s)	1.2			Normalised electron thermal diffusivity		
	$\chi_{i\perp}/n_i$ (m^2/s)	1.2 ∀i			Normalised ion thermal diffusivity		

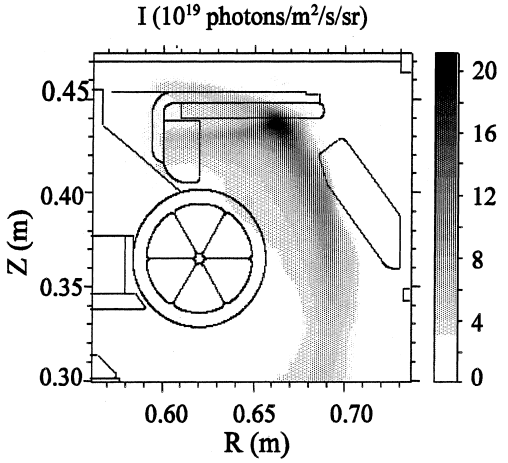

Fig. 5. Measured specific intensity for $n_0 = 2.33 \times 10^{19}$ m^{-3}.

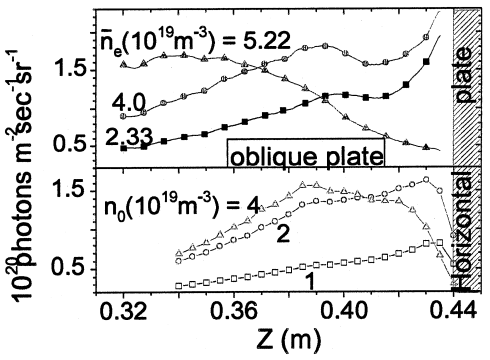

Fig. 6. Comparison between the measured (full) and calculated (open) D_α specific intensity in the outer divertor. In each case, the maximum intensity found in a horizontal plane is plotted as a function of the plane Z coordinate.

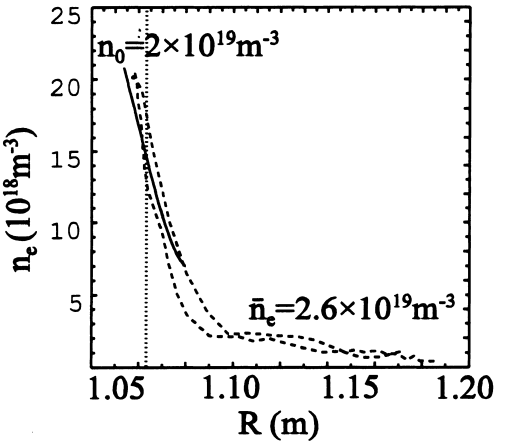

Fig. 7. Comparison between the calculated (solid) and measured (dashed) density profiles in the outer midplane. The vertical dotted line indicates the position of the separatrix.

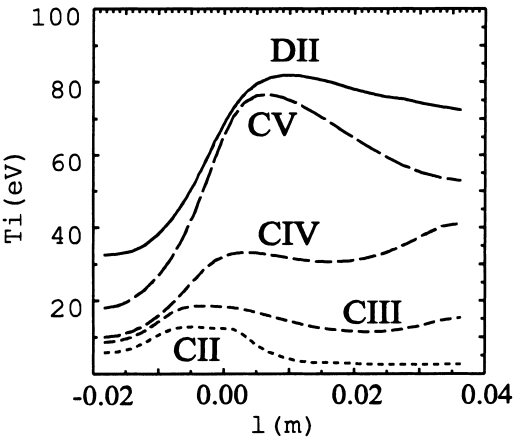

Fig. 8. Ion temperature profiles in the outer divertor along a horizontal path, 35 cm above the midplane calculated with $n_0 = 2 \times 10^{19}$ m^{-3}, $T_0 = 150$ eV. $l = 0$ corresponds to the position of the separatrix.

centre, towards the edge, of approximately 180 kW. Here also, the correspondence between the boundary condition n_0 and the measured line average density $\bar{n}_e$ is uncertain and a quantitative comparison is therefore not attempted. As an example, the density profile calculated in the midplane with $n_0 = 2 \times 10^{19}$ m^{-3} is compared in Fig. 7, with the measured density profile, for a line average density of $\bar{n}_e \sim 2.6 \times 10^{19}$ m^{-3}. As for the TdeV95 geometry, the good agreement found here suggests that $\bar{n}_e \sim 1.3 \times n_0$.

We now turn to the assessment of the validity of the single ion temperature approximation, frequently made in modelling impurity transport. First, a low density plasma is considered in Fig. 8, corresponding to $n_0 = 1 \times 10^{19}$ m^{-3}. In this figure, ion temperatures are plotted for every ion species considered in the simulation, along a horizontal path across the outer divertor, 0.35 m above the midplane (dashed line in Fig. 2). These profiles show significant differences between the temperatures of the various ion species. As expected, the lower ionisation stages of carbon have a lower temperature. This is due, in part, to the stronger coupling of low ionisation stages with (cold) neutrals produced by sputtering. It is also related to the stronger (Z^2) coupling of higher ionisation stages with deuterium ions. Except for DII and CV which are nearly at the same temperature where the plasma density is significant, it appears that a single ion temperature approximation would not be adequate in this case. Similar results are presented in Fig. 9 for a higher density ($n_0 = 4 \times 10^{19}$ m^{-3}). Here again, the carbon ion temperatures are found to increase with the ion charge. In this case,

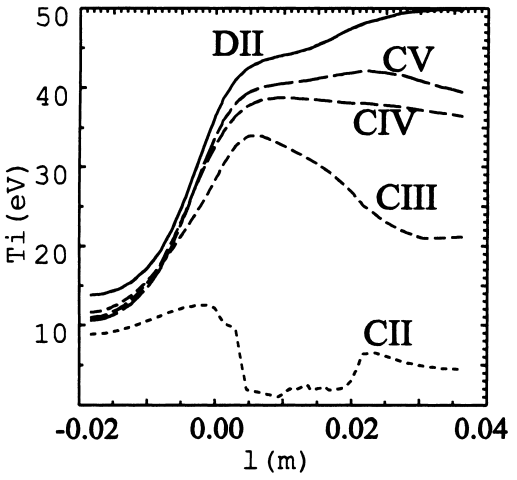

Fig. 9. Ion temperature profiles in the outer divertor, along a horizontal path 35 cm above the midplane, calculated with $n_0 = 4 \times 10^{19}$ m^{-3}, $T_0 = 60$ eV. $l = 0$ corresponds to the position of the separatrix.

however, the single ion approximation may be adequate for the combined DII, CV and CIV ions. The proximity of the temperatures here is a consequence of the lower temperatures, and of the higher density, which both result in an increased ion-ion collision frequency. The single ion temperature approximation breaks down, however, for doubly and singly ionised carbon. These differences in ion temperature are consistent with an earlier Monte Carlo simulation results from Shimizu, et al. [10].

6. Summary and conclusion

Simulations have been made of plasma and impurity transport in two divertor geometries of TdeV. A particular attention has been given to the calculation of D_α emissivity and specific intensity profiles, for which detailed experimental measurements are available. A precise quantitative comparison between simulation results and experiment is difficult, mainly because of the uncertainty in relating boundary conditions used in the model, with line average densities determined in the experiment. The model is nonetheless able to reproduce intensity profiles which are quantitatively close to measured values. The general changes in the intensity profiles as the plasma density is increased, are also reproduced.

Individual ion temperatures in a deuterium plasma with sputtered carbon impurities have been calculated, for representative TdeV operating conditions. Contrary to the common assumption that all ion species are nearly at the same temperature, different ionisation stages of carbon are found to have significantly different temperatures. Because of their higher (Z^2) collisionality, the higher ionisation stages generally have a temperature which is closer to the dominant DII ions. Because of recycling, however, and because of the coupling between low ionisation stage ions with neutrals, the temperatures calculated for these ions are considerably less than that of DII. These differences raise a serious question concerning the very nature of the energy distribution of ions in the divertor region, which may be non Maxwellian. The study of the exact form of the distribution function and its effect on transport is beyond the scope of the present approach. Suffice it to say that any transport process in which ion temperature profiles are involved should be examined with caution.

Acknowledgements

This work was funded by the Government of Canada, Hydro-Québec, and the Institut National de la Recherche Scientifique.

References

[1] R. Schneider, D. Reiter, D. Coster, J. Neuhauser, K. Lackner, B. Braams, J. Nucl. Mater. 220–222 (1995) 1076.
[2] A. Taroni, G. Corrigan, R. Simonini, J. Spence, S. Weber, J. Nucl. Mater. 220–222 (1995) 1086.
[3] S. Tsuji, K. Shimizu, T. Takizuka, N. Asakura, K. Itami, M. Shimada, Y. Suzuki, N. Ueda, J. Nucl. Mater. 220–222 (1995) 400.
[4] G.R. Smith, P.N. Brown, R.B. Campbell, D.A. Knoll, P.R. McHugh, M.E. Rensink, T.D. Rognlien, J. Nucl. Mater. 220–222 (1995) 1024.
[5] R. Marchand, M. Simard, Nucl. Fusion 37 (1997) 1629.
[6] H.A. Claaβen, H. Gerhauser, R.N. El-Sharif, private communication (1997).
[7] G.J. Radford, JET report JET-R(93)05 (1997).
[8] S.I. Braginskii, In: M. Leontovich, (Ed.), Reviews of Plasma Physics, Consultants Bureau, New York, vol. 1, (1965) p. 205.
[9] R. Marchand, C. Illescas, X. Bonnin, J. Botero, International Atomic Energy Agency, INDC(NDS)-309 (1995).
[10] K. Shimizu, T. Takizuka, A. Sakasai, J. Nucl. Mater. 241–243 (1997) 167.